Acta Crystallographica Section B
Structural Science
ISSN 0108-7681

On the charge transfer between conventional cations: the structures of ternary oxides and chalcogenides of alkali metals

Angel Vegas

Universidad de Burgos, Parque Científico y Tecnológico, Edificio I+D+I, Plaza Misael Bañuelos, s/n, 09001 Burgos, Spain, and Instituto de Química Física 'Rocasolano', CSIC, Madrid, Spain

Correspondence e-mail: avegas@iqfr.csic.es

Received 20 April 2012
Accepted 10 May 2012

Dedicated to Professor Sten Andersson on the occasion of his 80th birthday

...when I arrived you were gone

The structures of ternary oxides and chalcogenides of alkali metals are dissected in light of the extended Zintl–Klemm concept. This model, which has been successfully extended to other compounds different to the Zintl phases, assumes that crystal structures can be better understood if the cation substructures are contemplated as Zintl polyanions. This implies the occurrence of charge transfer between cations, even if they are of the same kind. In this article, the charge transfer between cations is even more illustrative because the two alkali atoms have different electronegativity, so that the less electropositive alkali metal and the O/S atom always form skeletons characteristic of the group 14 elements. Thus, partial structures of the zincblende-, wurtzite-, PbO- and $SrAl_2$-type are found in the oxides/sulfides. In this work, such an interpretation of the structures remains at a topological level. The analysis also shows that this interpretation is complementary to the model developed by Andersson and Hyde which contemplates the structures as the intergrowth of structural slabs of more simple compounds.

1. Introduction

The importance of the classical cation arrays in determining the structure of inorganic compounds has been highlighted in the last 40 years. From the pioneering observation of Wondratschek *et al.* (1964), followed by the works of Lebedev (1972) and Borisov (2000), up to the systematic study carried out by O'Keeffe & Hyde (1985), later extended by Vegas and co-workers (Martínez-Cruz *et al.*, 1994; Vegas, 2000; Santamaría-Pérez & Vegas, 2003; Vegas & García-Baonza, 2007; Vegas *et al.*, 2009; Vegas, 2011*a*) and also by Blatov and co-workers (Ilyushin *et al.*, 2004; Blatov & Peskov, 2006; Blatov, 2009, 2011), the classical idea of the structures thought of as isolated cations inserted into anionic networks has been questioned.

The main reason for this controversy comes from the fact that the classical vision of the structures, which is unable to account for the precise sites occupied by the cations in their respective anionic matrices, contradicts the most recent observations indicating that cations are not located at unplanned sites but they reproduce the structures of simple alloys (Wondratschek *et al.*, 1964; O'Keeffe & Hyde, 1985; Vegas, 2011*a*; Blatov, 2011). Moreover, in many instances the cation arrays are simply the structures of their own elements/alloys. The pairs $Sr_5As_3/Sr_5As_3O_{12}Cl$, $BaSn/BaSnO_3$, Si/SiO_2 (cristobalite), HP-Na_2S/HT-Na_2SO_4, *etc.* clearly illustrate that, in the oxides, cations try to maintain their own structure in spite of the presence of anions. In connection with this, we must mention the theoretical calculations, carried out on the Al-skeletons existing in the AlX_3 trihalides (Vegas *et al.*, 2006),

showing that the Al-substructures were thermodynamically and mechanically stable entities. An analysis of the electron density also showed the existence of bonding-critical points between the Al atoms, with directed Al—Al bonds.

These features confirm the hypotheses of the AMM (anions in metallic matrices) model which regards the crystal structure of many inorganic compounds as resulting from a metallic matrix acting as a host lattice for non-metallic atoms, the electron density of the metal inducing the final positions of the non-metallic atoms in the crystal. The AMM model justifies the observations of O'Keeffe & Hyde (1985) and explains the relevant role played by the metallic electron density.

A comprehensive survey on this fact can be found in the articles by Vegas & Jansen (2002), Vegas *et al.* (2009), Vegas & Mattesini (2010) and Vegas (2011*a*). These studies did not aim to establish mere relationships between alloys and oxides but it has led to new and unexpected relationships between oxidation and pressure and how the pressure induced by the O atoms can be overcome at high temperature. Thus, the composition–pressure–temperature space acquires a true physical and chemical sense also accounting for the phase transitions undergone by alloys and oxides (Vegas, 2011*a*).

A controversial aspect of our works has been the generalization of the Zintl–Klemm concept (Zintl, 1939) reported in Santamaría-Pérez & Vegas (2003), Santamaría-Pérez *et al.* (2005), Vegas & García-Baonza, (2007) and Vegas *et al.* (2009). As shown in these articles, this concept, applied classically to the Zintl phases, can also account for the skeletons of the polyanions such as aluminates, silicates, phosphates *etc.* when the concept is applied to their cation arrays, an idea that was firstly envisaged by Parthé and co-workers (Parthé & Engel, 1986; Parthé & Chabot, 1990). Thus, if in a given silicate, like $BaSiO_3$, the O atoms are neglected, one obtains the formula of the Zintl phase BaSi, in which the expected connectivity of the Zintl polyanion coincides with that of the Si atoms in the silicate.

In the articles concerning aluminates and silicates (Santamaría-Pérez & Vegas, 2003; Santamaría-Pérez *et al.*, 2005) it was highlighted that the Al atoms could show the same amphoteric character in crystals as shown in solution, so the Al atoms coordinated octahedrally with O would act as donor atoms whereas those coordinated tetrahedrally would act as charge acceptors, thus forming the tetrahedral skeletons which underlie the Zintl polyanions. This idea, regarding the possibility of charge transfer between atoms of the same kind, was later applied successfully to the silicate structures (Santamaría-Pérez *et al.*, 2005). In more recent articles (Vegas & García-Baonza, 2007; Vegas *et al.*, 2009) we have shown that the same idea can be applied to structures containing alkali metals or even transition metals, in which the charge transfer between Li, Na, K or Co, Mn atoms allows for a simple rationalization of their structures.

We must recognize that this uncommon viewpoint might well provoke dissension among crystal chemists. Thus, in $CsLiSO_4$ the one-electron transfer from Cs to Li to yield the four-connected Ψ-BeS [(II)–(VI)] network (Vegas & García-Baonza, 2007) could be accepted in view of the different electronegativity of Cs and Li. However, similar charge transfers between Na atoms in, for example, HP-Na_2S, might be much more disputable.

In this work we have analysed the structures of the ternary oxides and chalcogenides of alkali metals. The study reveals that in all cases the less electropositive alkali metal atoms form with the O/S atom networks which can be seen as Zintl polyanions. The most electropositive alkali atom acts as a donor and the complete structure can be explained in terms of the extended Zintl–Klemm concept (Santamaría-Pérez *et al.*, 2005; Vegas & García-Baonza, 2007; Vegas *et al.*, 2009).

2. Ternary oxides

Structural data have been reported for the ternary oxides KLiO, KTlO, NaRbO, LiRbO and NaTlO, and have been taken from *Pearson's Crystal Data* (Villars & Cenzual, 2008/9) and the ICSD (Inorganic Crystal Structure Database, 2010). The first comparison should be made with the binary oxides M_2O (M = Li, Na, Rb, Cs) which, with the exception of Cs_2O, are of the anti-fluorite type. It has been discussed elsewhere (Vegas *et al.*, 2009) that a fluorite-type structure could also been interpreted as a filled zincblende structure if we assume charge transfer between the two M atoms. This hypothesis, which is difficult to verify experimentally in binary oxides, will be better illustrated in ternary compounds, as shown below.

2.1. KLiO

The structure of KLiO was reported by Sabrowsky, Mertens & Dönhoff (1985). It is orthorhombic (*Cmca*, Z = 8) and is represented in Fig. 1(*a*). It consists of planar $\mathbf{4{\cdot}8^2}$ nets formed by Li and O atoms that are located at $x = 0, \frac{1}{2}$. These layers are intercalated by double $\mathbf{4^4}$ nets of K atoms which reproduce almost exactly the (100) faces of f.c.c.-K (face-centred cubic; stable in the range 11.6–23 GPa; Winzenick *et al.*, 1994; 6.40 × 6.42 Å in KLiO and 6.57 Å in high-pressure K). Regarding the LiO $\mathbf{4{\cdot}8^2}$ planar nets, one of them has been isolated in Fig. 1(*c*). The three Li—O distances are 1.896, 1.870 and 1.908 Å (mean 1.891 Å) and the Li—O—Li angles have values of 127.12, 126.49 and 106.39° (mean 120°) in agreement with the observed planarity shown in Fig. 1(*d*).

If the extended Zint–Klemm concept (EZKC) is applied to KLiO, it can be assumed that the more electropositive K atom donates its valence electron to Li, thus converting the LiO moiety into $[LiO]^-$ which is isoelectronic to BeO so that, after the Zint–Klemm concept, $[LiO]^-$ can be reformulated as [Ψ-BeO]. Since the $\mathbf{4{\cdot}8^2}$ nets are completely planar, the system might be considered as an aromatic II–VI compound which adopts a conformation equivalent to the graphene-like structure of BN [(III)–(V)] or the own carbon (graphite), a (IV)–(IV) compound. A more regular, completely planar $\mathbf{4{\cdot}8^2}$ net is formed by the BC subarray in CaB_2C_2 (Albert & Schmitt, 1999), as shown in Fig. 1(*b*). The aromaticity of the $[LiO]^-$ network and its relationship with the analogous graphite-like BN has already been advertised by Sabrowsky *et al.* (1985).

Even if the features described above are of great interest, other similarities give additional support to our hypothesis. Thus, in the same manner that carbon [(IV)–(IV)] can form the aromatic, two-dimensional, $\mathbf{6^3}$ layers of graphene as well as three-dimensional, four-connected networks like in diamond and londsdaleite, the (II)–(VI) compounds can also adopt different frameworks. One can find either three-dimensional networks like in zincblende, wurtzite and β-BeO (also in mineral variscite $AlPO_4{\cdot}2H_2O$) or in aromatic planar structures like graphene and KLiO. Recall that BeO (beryllia) is wurtzite-type (londsdaleite-like) at ambient conditions and transforms at 2373 K into the β-BeO phase (Smith *et al.*, 1965). This tetragonal phase ($P4_2/mnm$) forms the singular three-dimensional four-connected network represented in Fig. 2. The planar $[LiO]^-$ sheets (Ψ-BeO) of Fig. 1(*d*) lead to speculation about the existence of an aromatic carbon analogue.

As can be seen in Fig. 2(*a*), the β-beryllia structure presents similarities with that of KLiO (see Fig. 1*a*). They have the existence of $\mathbf{4{\cdot}8^2}$ nets in common. However, the differences are obvious. In β-BeO the fourfold connectivity obligates the $\mathbf{4{\cdot}8^2}$ nets to be strongly puckered instead of the planarity exhibited in KLiO. The structures also differ in the stacking of the $\mathbf{4{\cdot}8^2}$ nets which are eclipsed in β-BeO (compare Figs. 1*a* and 2*a*).

As discussed earlier (Santamaría-Pérez & Vegas, 2003; Vegas & García-Baonza, 2007; Vegas *et al.*, 2009), the structure of β-BeO (II)–(VI) also appears in (III)–(V) compounds like in the mineral metavariscite $AlPO_4{\cdot}2H_2O$ whose AlP substructure is represented in Fig. 2(*b*). However, interest is greater when we see that $AlPO_4{\cdot}2H_2O$ has another polymorph (the mineral variscite) whose AlP substructure also forms a

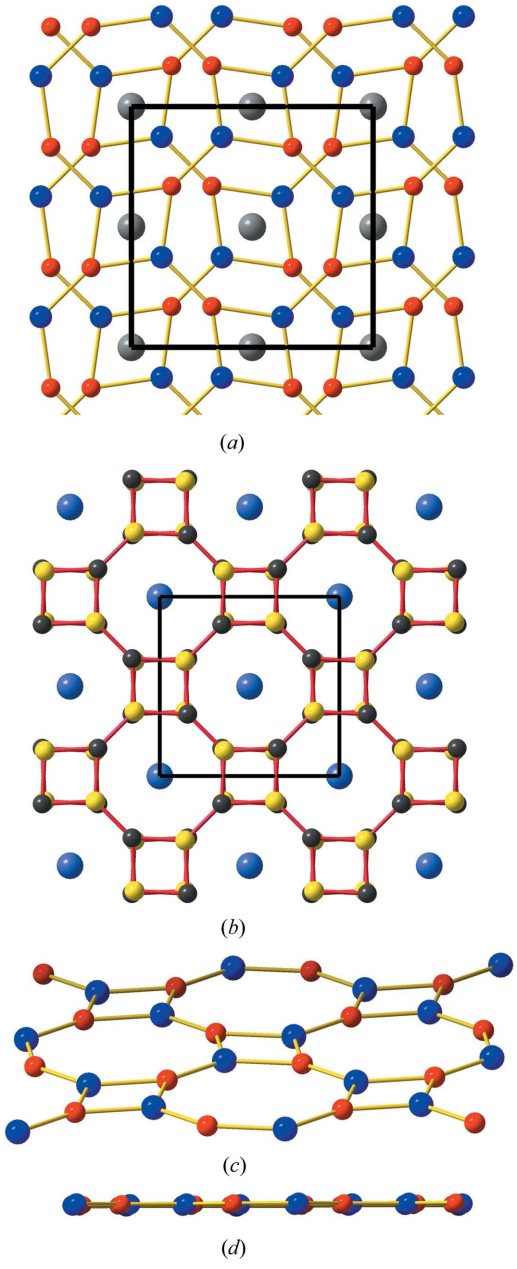

Figure 1
The tetragonal structure of KLiO (K: grey; Li: blue; O: red). (*a*) The structure projected on the *bc* plane showing the $\mathbf{4{\cdot}8^2}$ planar nets formed by Li and O atoms, stacked in the $\ldots ABAB\ldots$ sequence. These planar nets are intercalated with double layers of K atoms that reproduce the (100) planes of the f.c.c. structure of HP-K. (*b*) The related structure of CaB_2C_2 showing the tetragonal symmetry of the C_2B_2 planar nets that in this case are stacked in an eclipsed array. (*c*) Perspective view of one of the LiO layers whose planarity is shown in (*d*).

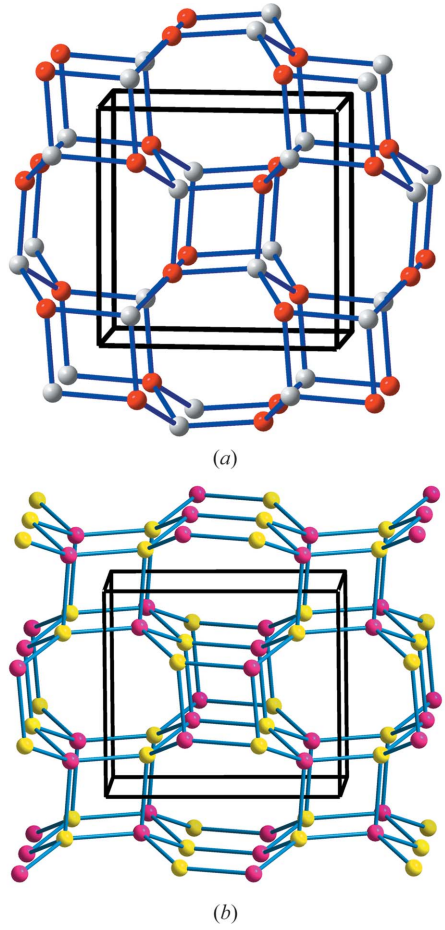

Figure 2
(*a*) Perspective view of the four-connected structure of β-BeO structure (Be: grey; O: red). The similar structure of the AlP subarray of metavariscite $AlPO_4{\cdot}2H_2O$ (P: purple, Al: yellow; O atoms and water molecules are omitted).

three-dimensional four-connected network containing the same puckered $\mathbf{4{\cdot}8^2}$ nets but, in this case, stacked in an ...*ABAB*... sequence as occurred in KLiO. The AlP array of variscite is represented in Fig. 3(*a*) which should be compared with the Ψ-BeO array of KLiO of Fig. 1(*a*).

One of these puckered layers, common to both variscite and metavariscite, has been drawn in Fig. 3(*b*) to show its similarity with the planar net of Fig. 1(*c*). The important issue here is that if the K atoms were ideally taken out from KLiO, in Fig. 1(*a*), the structure would collapse producing either the aromatic graphene analogue of BeO with threefold connectivity or the four-connected variscite analogue of *β*-BeO. Note that the analogies with graphene only refer to their planarity not to their geometry, $\mathbf{6^3}$ and $\mathbf{4{\cdot}8^2}$ for graphene and KLiO, respectively.

2.2. RbNaO

The structure of RbNaO is anti-PbFCl-type (*P*4/*nmm*, *Z* = 2) as reported by Sabrowsky, Vogt-Mertens & Thimm (1985).The structure, also known as of the Cu_2Sb-type, is common in binary compounds and has been widely studied because it also occurs in Zintl phases such as NaAlSi. In this last case, the $[AlSi]^-$ subarray, following the Zintl–Klemm concept (Santamaría-Pérez *et al.*, 2005), can be reformulated as Ψ-Si. As expected, the Ψ-Si partial structure is four-connected and is also isotypic to the related BiIn and PbO compounds (III)–(V) and (II)–(VI). The ternary oxides and chalcogenides KNaO, NaLiS, KLiS, RbLiS and CsNaTe, as well as the related KAgSe are also isotypic to RbNaO.

The structure is represented in Fig. 4(*a*), projected on the *bc* plane, whereas that of the isostructural KLiS is drawn in perspective in Fig. 4(*b*). As can be seen, the NaO (LiS) partial

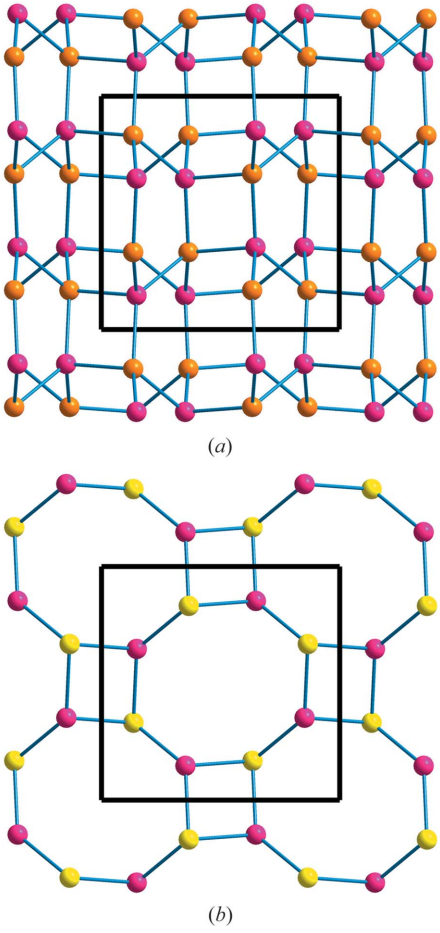

Figure 3
(*a*) The AlP subarray of $AlPO_4{\cdot}2H_2O$ (variscite) showing the three-dimensional network formed by the puckered $\mathbf{4{\cdot}8^2}$ nets stacked in an ...*ABAB*... sequence. One of the puckered layers has been isolated in (*b*). Compare with the drawings of Fig. 1. P: purple; Al: yellow; O atoms and water molecules are omitted.

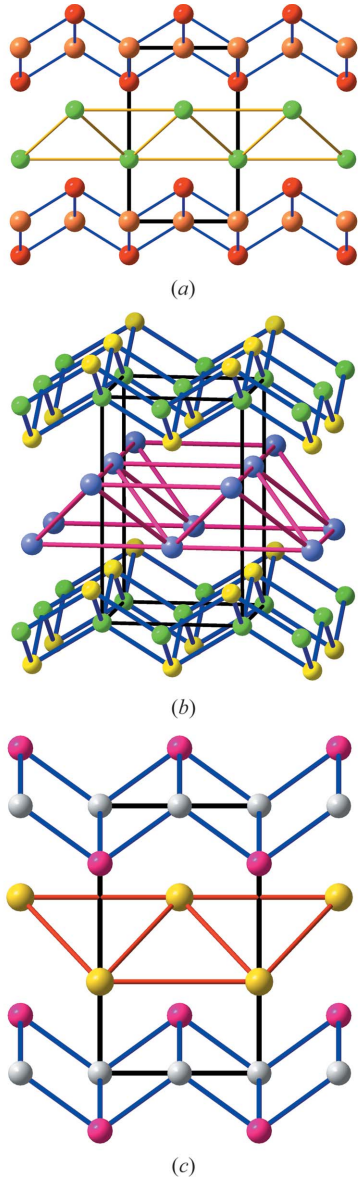

Figure 4
(*a*) The structure of RbNaO showing the PbO-type blocks of the $[NaO]^-$ moiety separated by blocks of Rb atoms. Na: light brown; O: red; Rb: green. (*b*) Perspective view of the KLiS structure showing the fourfold connectivity of the Li and S atoms. The Ψ-BeS blocks are separated by K blocks showing a b.c.c. topology. Li: green; S: yellow; K: dark blue. (*c*) The structure of KAgSe whose $[AgSe]^- \equiv$ Ψ-CdSe array is also of the PbO type. Ag: light grey; Se: purple; K: yellow.

structures form four-connected bidimensional slabs, separated by layers of Rb (K) atoms. The basic features of that array are the tetrahedral coordination of the NaO_4 (LiS_4) groups, whereas the O atoms are capping the squares of the $\mathbf{4^4}$ planar nets formed by the Na (Li) atoms.

The four-connected network formed by NaO (LiS) provides an explanation in the context of the EZKC. Thus, the one-electron transfer from Rb (K) to the NaO (LiS) substructure would give the pseudo-compounds Ψ-[MgO] and Ψ-[BeS], respectively, again (II)–(VI) pairs forming structures isotypic to (IV)–(IV) compounds. This argument could be seen as weakly founded in the case of the Ψ-[MgO] structure because real MgO is only known as rocksalt- and CsCl-type.

However, if Ψ-[BeS] is used as a reference, the PbO-type structure should be expected because it is considered as an intermediate step in the zincblende → rocksalt transition under pressure (Catti, 2005). Recall that BeS is zincblende at ambient conditions (Staritzky, 1956). This important relationship finds support in the different phases known for FeS. Among others, zincblende, PbO-type (stable below 540 K) and NiAs-type have been reported. CuI also undergoes the zincblende → PbO transition above 4.7 GPa (Hofmann *et al.*, 1995). In the related selenide KAgSe, the assumption of one-electron transfer from K to Ag to yield Ψ-[CdSe] could also be justified by the ZnS → NaCl phase transition observed at 3.2 GPa in CdSe itself (Mariano & Warekois, 1963). In this last case, however, the intermediate PbO-type phase has not been reported. The structure is factually a PbO-type (or BiIn-type) structure whose slabs are separated by the Rb layers which are the atoms that provoke the formation of the PbO-type slabs.

The stabilization of the $[NaO]^-$ (Ψ-[MgO]) fragments with PbO-type structure, which would correspond to a hypothetical HP phase of MgO (Catti, 2005), can also be justified by the fact that the formation of RbNaO takes place with a volume contraction close to 14% with respect to the sum of the individual Na_2O and Rb_2O anti-fluorite structures (Sabrowsky, Vogt-Mertens & Thimm, 1985).

Another interesting feature is that the dimensions of both the $[NaO]^-$ blocks and the anti-fluorite Na_2O structure are almost coincident. Thus, the yellow unit cell in RbNaO, depicted in Fig. 5(*a*), is a = 5.75 and 5.55 Å in the anti-fluorite Na_2O. In the same way, the Na—Na and Na—O distances are 2.877 and 2.395 Å in RbNaO compared with the values of 2.77 and 2.40 Å in Na_2O. The way in which the PbO-type fragments can be derived from the fluorite-type structure is illustrated in the series of drawings collected in Fig. 5. Note that the PbO-

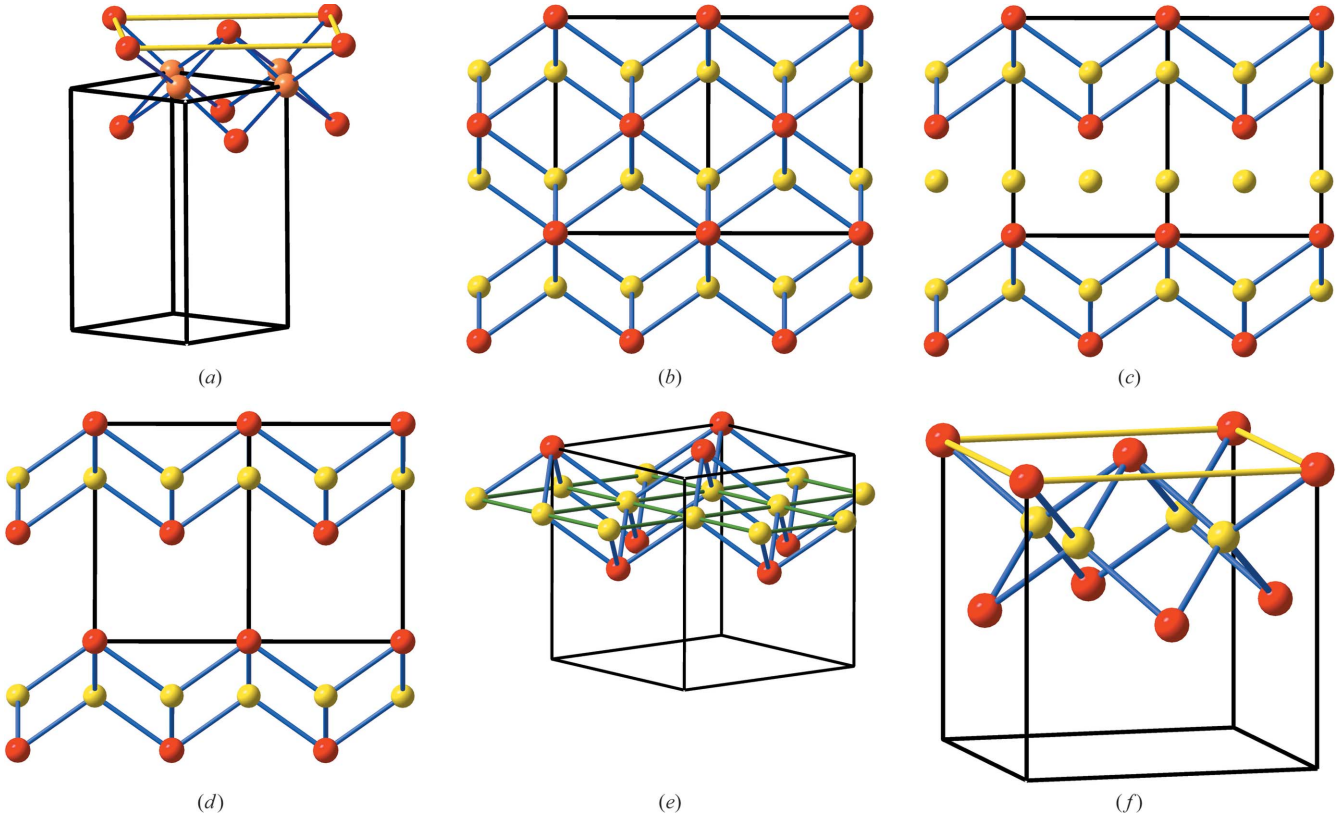

Figure 5
(*a*) A perspective view of a fragment of the NaO partial structure in RbNaO drawn in Fig. 4(*a*). A fragment of the PbO-type structure has been selected to illustrate its similarity with the anti-fluorite structure. It contains the (001), (002) and (004) planes. The hypothetical unit-cell edges are marked in yellow. Na: light brown; O: red. (*b*) The antifluorite structure of Na_2O, viewed along [110] to show that the PbO-type structure is implicit. Na: yellow; O: red; Na—O contacts: blue. (*c*) The same figure but the central Na—O contacts have been omitted to highlight the two PbO-type fragments. (*d*) The same drawing in which the central plane of the Na atoms has been eliminated to show the two PbO-type fragments preserved in RbNaO. (*e*) A perspective view of the upper block to show the fourfold connectivity of both Na and O atoms. (*f*) One half of the unit cell of Na_2O to show its identity with the same fragment in RbNaO drawn in (*a*).

type blocks are half of the anti-fluorite-type unit cell of Na_2O. They are formed by the (001) (yellow contacts) and (002) planes of O atoms plus the (004) planes formed only by Na atoms.

It should be added that the Rb fragments also show high-pressure effects. Thus, the two $\mathbf{4^4}$ Rb layers of RbNaO, with dimensions of 4.068 Å, are in fact (001) faces of a f.c.c.-net of a = 5.75 Å. This value only deviates 5% from the unit-cell dimension (a = 5.42 Å) of f.c.c.-Rb at 9 GPa (Takemura & Syassen, 1982). Since rubidium undergoes the b.c.c.–f.c.c. (base-centred cubic) transition at 7 GPa, it is expected that, at the transition pressure, the unit-cell parameter would be even closer to that found in RbNaO.

In the case of KLiS (Fig. 4*b*) the K bilayers correspond to fragments of a b.c.c.-net consisting of both (001) and (002) crystallographic planes. The unit-cell dimension is a = 4.32 Å yielding the shortest K—K distance of $a \times \sqrt{3}/2$ = 3.74 Å, almost equal to the value of 3.77 Å observed in the potassium metallic structure. Since the unit-cell dimensions of b.c.c.-K at the transition pressure (b.c.c. → f.c.c.) is greater than 4.32 Å, the K-blocks should be better regarded as (001) planes of f.c.c.-K whose unit cell would be $4.32 \times 2^{1/2}$ = 6.11 Å, comparable to the measured value of 6.57 Å at the transition. The important issue is, however, that the two layers are packed so as to produce an unexpected b.c.c. topology consisting of one half of its unit cell.

2.3. The related compound $CsLiCl_2$

When this article was written, the unique reference to this compound was the tetragonal phase (*P*4/*nmm*), synthesized by Gaebell *et al.* (1983), which is represented in Fig. 6. After submission, we were aware of the recent work by Pentin *et al.* (2012) reporting on the existence of a new monoclinic polymorph (*C*2/*c*; $CsLiF_2$-type) as well as on the structural transition between them.

Although this halide does not belong to the family of compounds considered in this article, the reasons for its inclusion here are twofold: On one hand it also contains blocks of the PbO-type which, as in RbNaO, are formed by the Li–Cl pair of atoms. On the other hand, the presence of the Cl atoms provides the ideal conditions to test the validity of the EZKC.

The structure is of the $BaNiS_2$-type and regardless of the stoichiometry, the structure has strong similarities to that of RbNaO or any of its isotypic compounds, such as KNaO, NaLiS, KLiS, RbLiS and CsNaTe. As can be observed in Fig. 6(*a*), the Li–Cl pair of atoms forms blocks of the PbO-type. These blocks are intercalated with a double layer of the composition CsCl, just one half of a distorted NaCl-type structure which is drawn separately in Fig. 6(*b*). Following the EZKC, the structure can be rationalized in the following way: The transfer of one electron from Cs to Li yields Li^- (Ψ-Be) and Cs^+. If, at the same time, the two Cl atoms disproportionate into Cl^+ and Cl^-, equivalent to Ψ-S and Ψ-Ar, respectively, then we could form a Ψ-BeS pair for which a PbO-type structure is expected and additionally a pair of Cs^+Cl^- with the distorted NaCl-type structure (see Fig. 6*b*).

We must recall that CsCl undergoes the CsCl → NaCl transition above 719 K (Schulz, 1951) and the important result here is that the halved CsCl partial structure has the dimensions 6.96 Å, coincident with the value of 6.94 Å observed experimentally for the unit-cell parameter of the rocksalt structure of CsCl.

It should be outlined that the aristotype $BaNiS_2$ is also coherent with this interpretation. Thus, the two-electron transfer from Ba to Ni would yield Ψ-ZnS with the PbO-type structure, intermediate in the zincblende → NaCl transition. On the other hand, if the electrons remain at the Ba atom, we have the rocksalt-type BaS moiety. Also here the dimensions of the BaS partial structure agree with those of BaS itself.

It could be argued that the structure could be interpreted as alternating blocks of LiCl and CsCl without the need for the application of the EZKC. In favor of this idea is the fact that the copper halides CuI and CuBr, usually related to the alkali halides, are PbO-type. In contrast we must outline that, among the alkali halides, only LiCl, LiBr and LiI (Bach *et al.*, 2009; Liebold-Ribeiro *et al.*, 2008; Wassermann *et al.*, 1988) have been obtained as metastable phases in a four-connected (wurtzite-type) network.

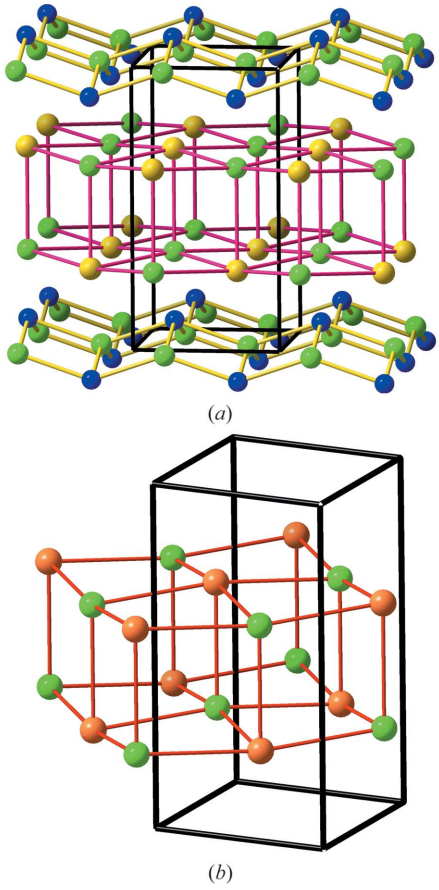

Figure 6
(*a*) Perspective view of the $CsLiCl_2$ structure to show the intergrowth of two structural blocks. The first one of composition LiCl adopting the PbO-type structure and the second one of composition CsCl consisting of one half of a unit cell of the NaCl type. Li: blue; Cl: green. (*b*) The distorted NaCl-type formed by the Cs–Cl atoms; Cs: brown; Cl: green.

2.4. KNaS and NaLiSe

The structures of these compounds are represented in Fig. 7. That of KNaS is drawn in perspective (Fig. 7*a*) to show the four-connected network of the NaS partial structure (Sabrowsky *et al.*, 1987). The analogous LiSe skeleton of NaLiSe (Bronger *et al.*, 1989) is drawn in projection in Fig. 7(*b*). As has been previously discussed (Vegas & García-Baonza, 2007), this four-connected network, characteristic of the Group 14 elements, corresponds to the Al-skeleton (Ψ-Si) in the Zintl phase $SrAl_2$. In our case the similarity is explained by the one-electron transfer from K to the Na atom, converting it into Ψ-MgS, a (II)–(VI) compound with a (IV)–(IV) network.

The same can be said of NaLiSe. The Na atom transfers its valence electron to the Li atom, converting it into Ψ-Be which forms the four-connected network with the Se atom. Again, a Ψ-(II)–(VI) compound is formed. As was previously pointed out (Vegas & García-Baonza, 2007; Vegas *et al.*, 2009), the charge transfer between atoms of the same kind has been postulated where possible. Thus, M^+ and M^- species might coexist in the same compound. Several experiments (Tinkham & Dye, 1985; Nakayama *et al.*, 1994; Terskikh *et al.*, 2001) have shown that such entities, *e.g.* potassides, could exist even in the solid state. Similarly, these ions might also coexist in other compounds, regardless of the fact that such entities could be (or not) identified in conventional diffraction experiments.

It should be remarked that KNaS can also be described as a ternary anti-cotunnite structure (anti-$PbCl_2$) which is found in the high-pressure phase of Na_2S and Rb_2S, and in the ambient pressure phase of Cs_2S (Vegas *et al.*, 2001; Sommer & Hoppe, 1977; Santamaria-Perez *et al.*, 2011). The same skeleton exists in the corresponding sulfates M_2SO_4 (O'Keeffe & Hyde, 1985; Vegas & García-Baonza, 2007). In some cases, like in KNaS, the structure is not isotypic with the corresponding $KNaSO_4$ sulfate, but with the room-temperature phase of K_2SO_4 (Pannetier & Gaultier, 1966). Our explanation, based on the EZKC, finds support in the fact that in all cases it is always the most electronegative atom (Li, Na) that forms the four-connected net with the S (Se) atom.

An additional example of charge tranfer between atoms of the same kind is provided by the related compound Ag_2Se ($P2_12_12_1$; Aliev & Aliev, 1989) represented in Fig. 8. The EZKC is derived into a Ψ-PdCdSe, where the [Ψ-CdSe] [(II)–(VI)] moiety forms the same structure as the Ψ-Si network in $SrAl_2$. Recall that real CdSe is wurtzite-type at ambient conditions but undergoes the wurtzite → zincblende transititon at 3.2 GPa (Mariano & Warekois, 1963).

2.5. LiRbO

The structure of LiRbO presents some singularities. It is represented in Fig. 9(*a*) and has been described as a variant of the KNaS structure described above (Sabrowsky & Vogt, 1987). Their apparent resemblance can be deduced by comparing Figs. 9(*a*) and 7(*a*). Their similarity resides in a

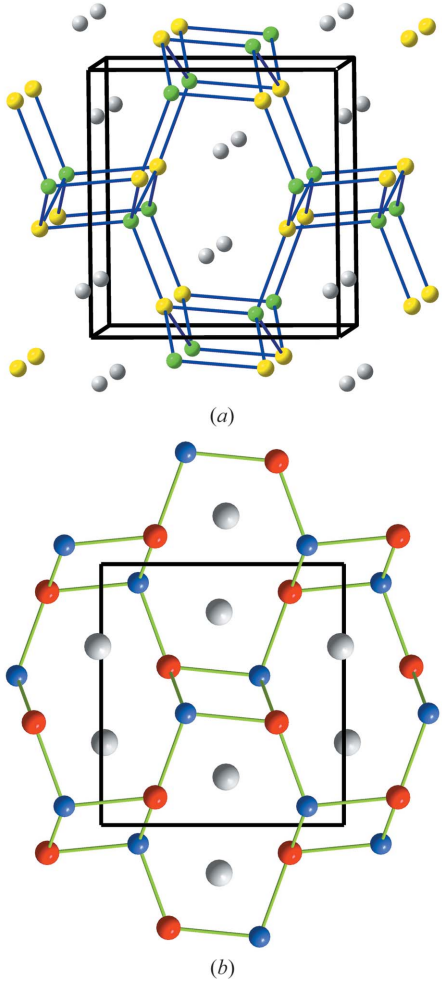

Figure 7
(*a*) Perspective view of the KNaS structure showing the four-connected network of the NaS partial structure. K: grey; Na: green; S: yellow. (*b*) Projection of the LiNaSe structure showing the similar structure of the LiS sub-array. Na: grey; Li: blue; Se: red.

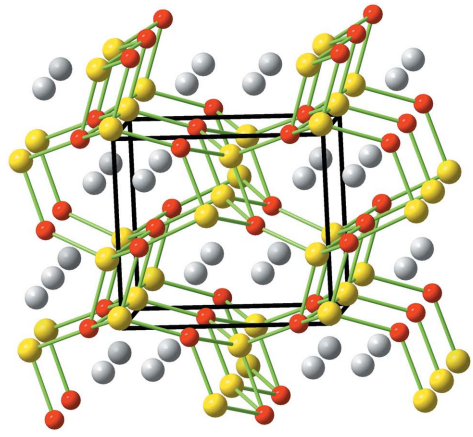

Figure 8
The structure of Ag_2Se in which one of the two crystallographically independent Ag atoms together with the S atom form the four-connected network of Ψ-Si in $SrAl_2$. Donor Ag atom: grey; acceptor Ag atom: yellow; Se: red. Compare with Fig. 7.

four-connected net formed by the Li and O atoms (see Fig. 9*a*) like that formed by the NaS partial structure shown in Fig. 7(*a*). However, the LiO partial structure is only four-connected if we take into account the three shortest Li—O distances, ranging from 1.89 to 1.97 Å, plus a fourth, extremely long distance of 4.02 Å.

The acceptance of physical meaning to the long contact seems problematic. So, when this longer contact is neglected, then the structure appears as a set of three-connected chains like those represented in Fig. 9*b*. These accordion-like blocks are similar to the Sb array in Sb_2O_3, so that it is more characteristic of a Group 15 element rather than of a Group 14 element (compound) as can be deduced by applying the EZKC, as done with KNaS (Fig. 7*a*).

Assuming the correctness of the structure determination we can see no reason for the structure to deviate so strongly from the expected regular structure. In fact, as said by the authors (Sabrowsky & Vogt, 1987) '. . . *it is surprising, that in view of the tendency for the threefold connectivity of Li with the O atoms, RbLiO is not isotypic with the new phase of KLiO*' (see Fig. 1). One possibility could be that this structure be a metastable phase in which the LiO partial structure is taking form to yield the undistorted network. However, this interpretation could be taken as poorly founded.

For this reason we have sought an alternative description that could account for this geometry. A new picture of LiRbO is projected on the *bc* plane (Fig. 10*a*). We have drawn the Rb–Rb contacts to outline the blocks of trigonal prisms of Rb atoms centred by the LiO pair of atoms. The blocks are displaced *a*/2 (the projection axis) with respect to each other. This array is a variant of the TlI-type structure which would interconvert by displacing the filled blocks by *c*/2 with respect to each other. This interpretation is meaningful when one sees

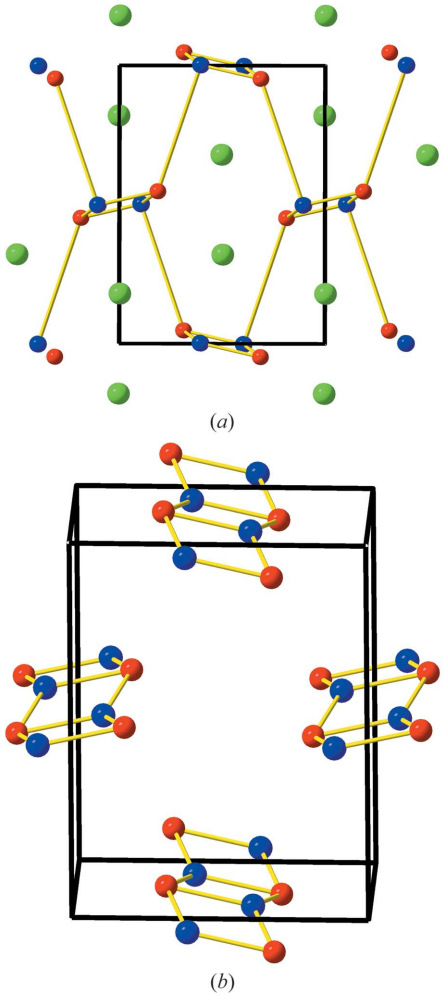

Figure 9
(*a*) The structure of RbLiO projected on the *ac* plane. Rb: green; Li: blue; O: red. The structure is a strong distortion of the $SrAl_2$-type structure like that represented in Fig. 7(*a*). (*b*) Perspective view of the three-connected accordion-like blocks formed by Li and O atoms when the longest contact is neglected.

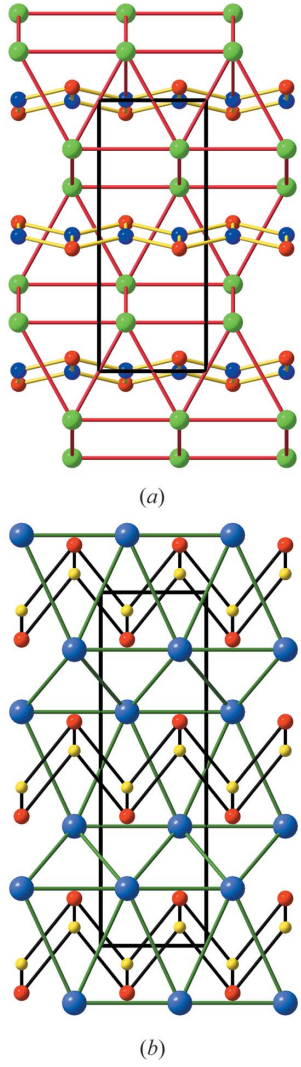

Figure 10
(*a*) The RbLiO structure projected on the *bc* plane. Rb: green; Li: dark blue; O: red. The Rb—Rb contacts (red lines) draw the trigonal prisms filled with the Li—O pairs. All the Li—O contacts are drawn with yellow lines. (*b*) The related structure of NaOH (*Cmcm*) of the TlI-type. Na: blue; O: red; H: yellow. The Na6 trigonal prisms are filled with the OH groups. Note the differences in the connection of the blocks of trigonal prisms.

that a similar structure is found for RbOH and also for NaOH, which is represented in Fig. 10(*b*).

The chemical resemblance is enhanced if we think that both the O—Li and O—H pairs have the same number of valence electrons (7*e*) and that they could be regarded as pseudo-halogens. In fact, compounds such as InCl, TlCl and InI are isotypic to RbLiO. It is noteworthy that in RbLiO the Li—O pairs are almost perpendicular to the projection axis, whereas in NaOH the hydroxyl groups lie on the projection plane. This different orientation indicates that the trigonal prisms are higher in RbLiO than in NaOH and therefore, the Li—O partial structure is almost prepared to form a PbO-type array.

2.6. Tl-containing compounds: KTlO and NaTlO

These Tl-containing oxides have been included because, in many instances, Tl^{I} behaves like an alkali metal. The monoclinic structure of KTlO (Sabrowsky, 1978) admits two interpretations. The first one is reflected in Fig. 11*a* and is based on bilayers of K and Tl atoms, which all together form a h.c.p. (hexagonal close packing) array, with all the octahedral voids filled by O atoms. The structure has strong similarities with the $CdCl_2$-type structure.

The second interpretation is based on the separation of the two cations K and Tl. If we connect the Tl and O atoms up to a distance of 2.5 Å, we obtain the pattern of Fig. 11(*b*) which contains accordion-like double chains like those isolated in Fig. 11(*c*). In these double chains the Tl and O atoms are alternating in such a way that all atoms are connected to three alike atoms. This kind of connection is characteristic of the structures formed by the Group 15 elements and, in fact, the network is similar to that of the Sb atoms in Sb_2O_3 (Svensson, 1974).

This three-connected skeleton can be rationalized by assuming the one-electron transfer from K to Tl, so the Tl—O partial structure becomes a pseudo [(IV)–(VI)] compound, equivalent to a three-connected network of the (V)–(V) compounds like that of Sb in Sb_2O_3. It is remarkable how both species of cations, *i.e.* K and Tl, even if they form octahedral layers altogether, they arrange inside the layer to simultaneously satisfy the structural requirements of the group 15 elements. It should be outlined that the same motif is formed by the K—O pair. However, we believe that it is more sensible to consider the Tl atom as the acceptor.

The second compound, NaTlO, is hexagonal (Sabrowsky, Mertens & Dönhoff, 1985) and the structure is represented in Fig. 12. The structure determination showed that the two cationic species are distributed randomly at the same Wyckoff site, forming regular octahedral layers which, like in KTlO, are filled by the O atoms.

Both structures are stacking variants of the $CdCl_2$ and CdI_2 structures. Recall that the binary oxide Cs_2O is also anti-$CdCl_2$-type (Helms & Klemm, 1939), in contrast with the remaining alkali oxides which are anti-fluorite. The results reported here indicate that electron transfer between Tl and alkali metals is less evident in these ternary oxides which adopt structures characteristic of very electropositive elements like Cs in Cs_2O.

2.7. The singular LiHS sulfide

Lithium hydrogen sulfide has been added to our study as an example of how the H atoms produce the same effect as other monovalent atoms in the structures. It crystallizes in several polymorphs (Jacobs *et al.*, 1989; Juza & Laurer, 1954; Winkler *et al.*, 2003). One of them ($P4_2/mmc$; Jacobs *et al.*, 1989) is isotypic to PtS and in the other two, crystallizing in the space group *Ama*2 and $P4_2/mbc$, the LiS-substructures are slight

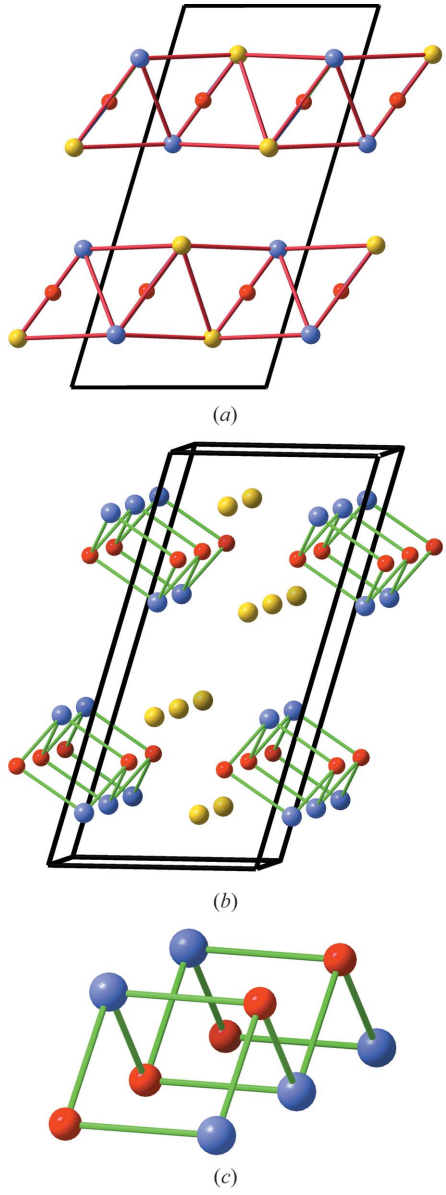

Figure 11
(*a*) The monoclinic structure of KTlO viewed along the *b* axis. K: yellow; Tl: blue; O: red. The K and Tl atoms form distorted octahedral layers filled by O atoms. (*b*) Perspective view of the same structure in which the Tl and O atoms have been connected. They form a folded double-chain structure with threefold connectivity like in Sb. (*c*) The accordion-like Tl—O double chains showing its three-connectivity and folding.

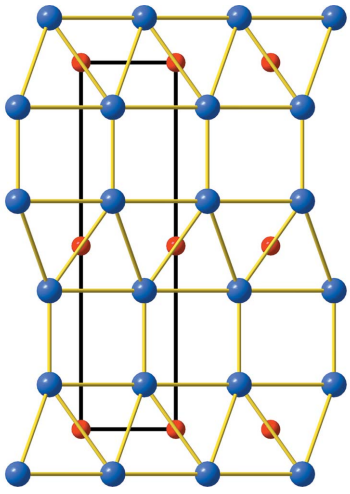

Figure 12
The hexagonal structure of NaTlO viewed along the *a* axis. Na/Tl: blue; O: red.

distortions of the PtS-type network, as shown in Figs. 13(*a*)–(*c*). The S atoms are linked to four Li atoms in a square-planar coordination, whereas the Li atoms are tetrahedrally coordinated by four S atoms. The result is the three-dimensional skeleton shown in Fig. 13(*b*).

Figs. 13(*a*)–(*c*) show that the three structures can be described as chains of Li atoms running along the projection axes. Their coordinating S atoms form Li_2S_2 squares which lie alternately perpendicular to each other, also resulting in the LiS_4 tetrahedra sharing edges which form the infinite chains of stoichiometry LiS_2. These LiS_2 chains have real chemical entities in compounds such as SiS_2, SiO_2, $CuCl_2$ and $BeCl_2$, and when adjacent chains condense, they yield the three-dimensional skeleton of the formula LiS which is shown in Figs. 13(*a*)–(*c*).

It is precisely the structure of $BeCl_2$ (Rundle & Lewis, 1952), projected in Fig. 13(*d*), which will serve as the starting point to explain the structure of LiHS. Thus, if in $BeCl_2$ two of the four Cl atoms surrounding the Be atoms were eliminated, then the chains would collapse into the pattern of Fig. 13(*a*). One of the indivual chains has been isolated in Fig. 13(*e*).

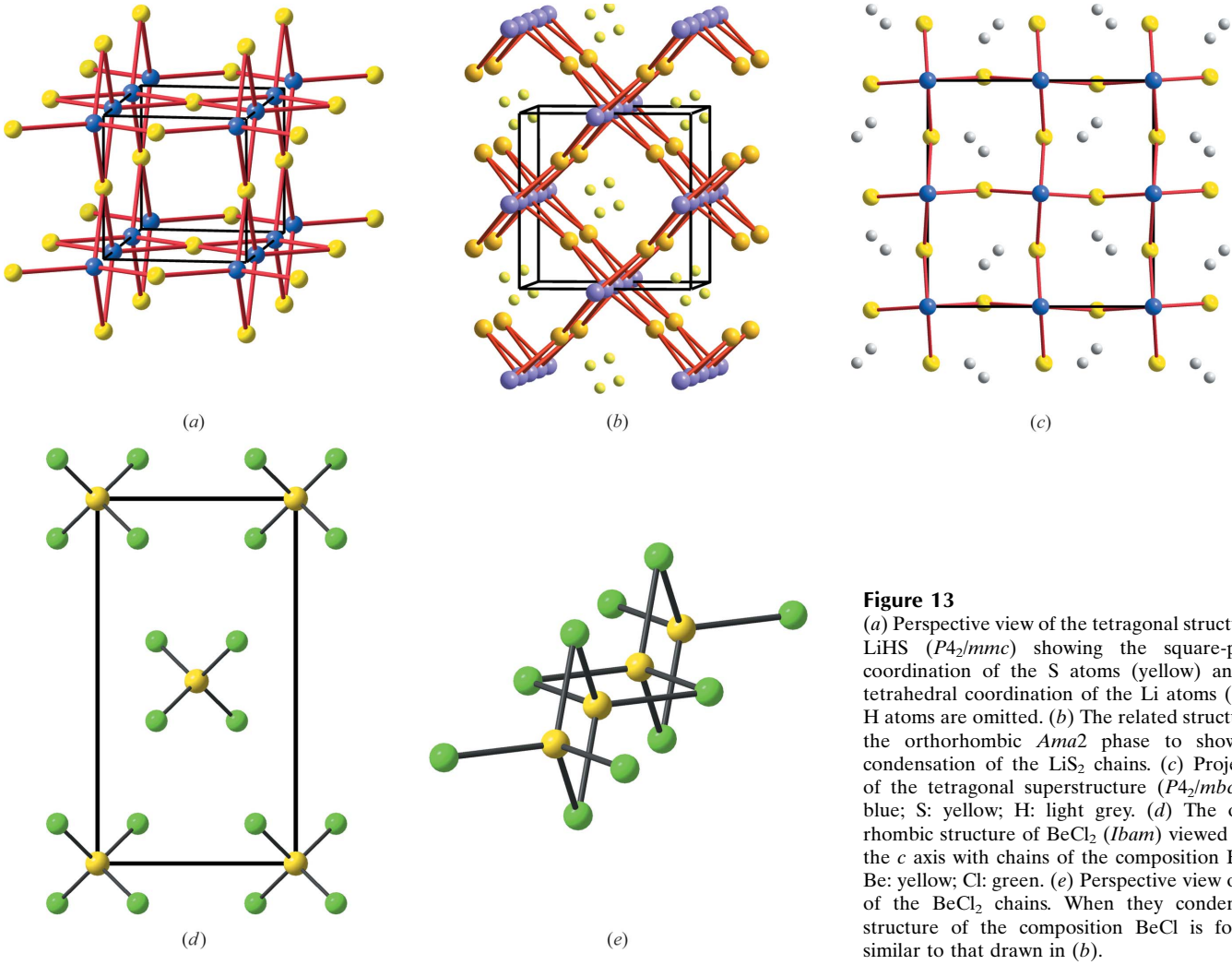

Figure 13
(*a*) Perspective view of the tetragonal structure of LiHS ($P4_2/mmc$) showing the square-planar coordination of the S atoms (yellow) and the tetrahedral coordination of the Li atoms (blue); H atoms are omitted. (*b*) The related structure of the orthorhombic *Ama*2 phase to show the condensation of the LiS_2 chains. (*c*) Projection of the tetragonal superstructure ($P4_2/mbc$). Li: blue; S: yellow; H: light grey. (*d*) The orthorhombic structure of $BeCl_2$ (*Ibam*) viewed along the *c* axis with chains of the composition $BeCl_2$; Be: yellow; Cl: green. (*e*) Perspective view of one of the $BeCl_2$ chains. When they condense, a structure of the composition BeCl is formed, similar to that drawn in (*b*).

The LiHS structure can then be rationalized in terms of the EZKC. Thus, the one-electron transfer from H to Li would convert the compound into Ψ-BeS, a pseudo-(II)–(VI) compound that, like ZnS or ZnO, produces four-connected networks (zincblende and wurtzite, respectively). This interpretation is tightly correlated with that of $BeCl_2$ because if in $BeCl_2$ we assume the transfer of one electron between the Cl atoms, we would obtain the formula $Cl^-[BeCl]^+$, equivalent to the pseudo-compound Ψ-Ar[Ψ-BeS] which contains the BeS structure if Ψ-Ar could be eliminated, *i.e.* if condensation would take place. Thus, the $BeCl_2$ structure (Fig. 13*d*) is well prepared to yield the BeS-type structure (Fig. 13*b*) if one Cl atom per formula is eliminated. Such a condensation process is illustrated in the sequence of drawings represented in Fig. 14.

It might be argued that the H atoms are tightly binded to the S atoms (S—H distances of 1.25 Å), making the transfer of its electron to the Li atom impossible. However, the electron might be transfered from the SH group acting as a whole. An alternative explanation is based on the SH groups being considered as pseudo-Cls, just like the hydroxyl groups are regarded as pseudo-halogens. This would lead to LiHS being described as pseudo-LiCl with a structure which can be explained as a condensed $CuCl_2$ structure.

The fourth phase of tetragonal symmetry (space group $I\bar{4}$) is represented in Fig. 15 (Juza & Laurer, 1954) and is directly related to the zincblende structure. It can be interpreted straightforwardly by using the arguments described above for the phases related to $BeCl_2$. Thus, assuming the same electron transfer from H to Li, the LiS pair would become Ψ-BeS, which, in this case adopts the ZnS-type structure of real BeS.

Also in this phase we can apply the equivalence LiHS ≡ pseudo-LiCl, accounting for the ZnS-type structure of LiHS, which is closely related to the ZnO-type metastable structure observed in LiCl (Bach *et al.*, 2009; Fischer *et al.*, 2004).

2.8. $LiAlSe_2$

The structure of $LiAlSe_2$ (Kim & Hughbanks, 2000) has also been selected because, even if it is not actually a ternary alkali selenide, containing only alkali metals, its structure presents some of the features previously described for other compounds. In addition, it has some singularities which can add to the understanding of other inorganic structures.

The structure is represented in Fig. 16 showing that when all atoms are connected a wurtzite-type (ZnO) structure is obtained. The reason for this array is that each LiAl pair contribute four electrons, an average of two electrons per atom. This means that the Li–Al pair could be averaged and considered as two Ψ-(Be/Mg) atoms which together with the two Se atoms yield either Ψ-BeSe or Ψ-MgSe compounds, two (II)–(VI) compounds that, like ZnSe, adopt a (IV)–(IV) array. This interpretation is an alternative way of expressing the EZKC and makes sense because BeSe itself is zincblende-type with a highly probable transition to wurtzite, as occurs with many other isotypic compounds. The existence of MgTe also with the ZnS structure gives more chemical sense to this interpretation.

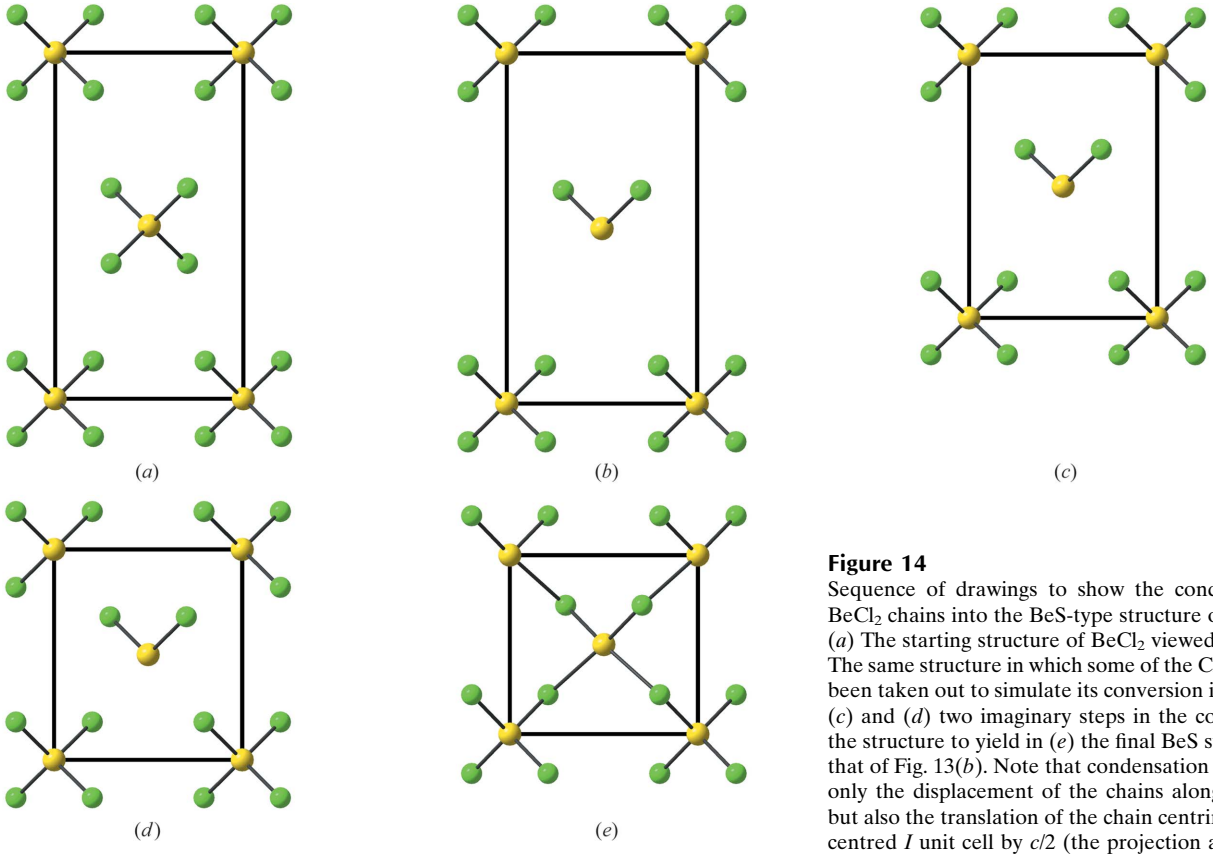

Figure 14
Sequence of drawings to show the condensation of $BeCl_2$ chains into the BeS-type structure of Fig. 13(*b*). (*a*) The starting structure of $BeCl_2$ viewed along *c*. (*b*) The same structure in which some of the Cl atoms have been taken out to simulate its conversion into S atoms. (*c*) and (*d*) two imaginary steps in the contraction of the structure to yield in (*e*) the final BeS structure like that of Fig. 13(*b*). Note that condensation involves not only the displacement of the chains along the *b* axis, but also the translation of the chain centring the body-centred *I* unit cell by *c*/2 (the projection axis).

As has been discussed with the bixbyites structure (Vegas *et al.*, 2009), $LiAlSe_2$ can also be interpreted as if one of the two Se atoms transferred one electron to the Li atom, so that $LiAlSe_2$ could be re-formulated as Ψ-[BeSe][AlAs] in which the two partial structures [BeSe] and [AlAs] correspond to real compounds that form ZnS- and ZnO-type skeletons.

It is important to mention here the existence of the compound $Al_{0.67}Se$, whose structure has been refined as a defective ZnO-type structure in which the Al atoms randomly occupy two thirds of the Zn positions in the wurtzite structure (Schneider & Gattow, 1954). This structure determination, from powder data, seems to be inaccurate. Although it is normal practice to consider these 'defects' as disordered, the question arises now about whether the structure under consideration ($LiAlSe_2$) could not be a model to reconsider the defect distribution in $Al_{0.67}Se$ which can also be formulated following the sequence $Al_{0.67}Se \equiv Al_{1.33}Se_2 \equiv Al_{0.33}AlSe_2 \equiv e^-AlSe_2 \equiv LiAlSe_2$.

This sequence of equivalences might lead to speculation that the voids occupied by Li atoms in $LiAlSe_2$ would correspond to the empty holes in the 'defective' $Al_{0.67}Se$ structure. If this was so, the defects would be ordered and, at the same time, occupied by electrons as shown in the above sequence. It could be argued that this speculation is weakly founded but consideration must be given to the high-pressure experiments carried out on elemental K (Marqués *et al.*, 2009) as well as the very recent study on aluminium by quantitative convergent-beam electron diffraction (QCBED; Nakashima *et al.*, 2011).

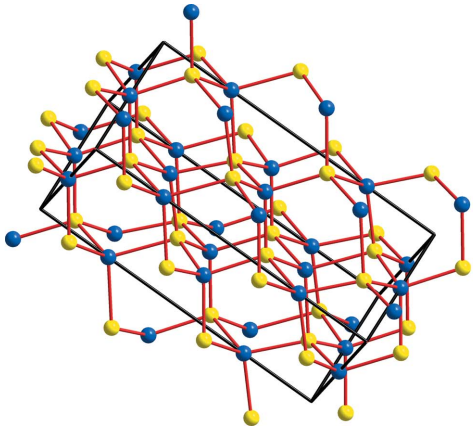

Figure 15
The LiS partial structure (Ψ-BeS) of the tetragonal ($I\bar{4}$) phase of LiHS. The structure is a tetragonal distortion of the zincblende structure of real BeS binary sulfide. Li: blue; S: yellow; H atoms are omitted.

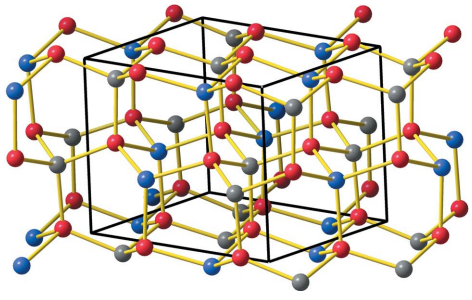

Figure 16
The distorted wurtzite-type structure of orthorhombic $LiAlSe_2$ ($Pna2_1$). Li: blue; Al: grey; Se: red.

In the first case, new high-pressure experiments have revealed the existence of a new hexagonal phase for elemental K. This phase is isotypic with the K substructure in the high-pressure phase of K_2S, which in turn also coincides with the same K partial structure in the high-temperature phase of K_2SO_4. Theoretical calculations (density functional theory, DFT, and electron localization function, ELF) have clearly shown that in high-pressure K the valence electrons are paired at the centre of the trigonal prisms which are just the sites occupied by either S and SO_4 groups in their respective compounds (Marqués *et al.*, 2009; Vegas & Mattesini, 2010). This localization of the valence electrons rationalizes the unexpected structural coincidences in K, K_2S and K_2SO_4.

In the case of aluminium, the accurate intensity measurements have permitted the calculation of reliable deformation density maps showing that the Al valence electrons are almost exclusively localized in the tetrahedral holes of the f.c.c.-Al core structure, in the same holes occupied by nominal anions such as N and P when they form the zincblende-type compounds AlN or AlP. Similar results were obtained from DFT calculations (Nakashima *et al.*, 2011).

It should be mentioned that ELF calculations carried out on CaO, CaF_2 and also on the pair BaSn/$BaSnO_3$ have shown that electrons, in the metal structures, are mainly located at the same positions occupied by the O atoms in the respective oxides, supporting the idea that electrons play the same role as anions and also giving chemical sense to the relationship between oxidation and pressure (Martínez-Cruz *et al.*, 1994; Vegas & Mattesini, 2010).

3. Concluding remarks

The results reported in this review validate the extension of the Zintl–Klemm concept (EZKC) to the cation arrays of alloys and oxides, as previously reported (Santamaría-Pérez & Vegas, 2003; Santamaría-Pérez *et al.*, 2005; Vegas & García-Baonza, 2007; Santamaría-Pérez & Liebau, 2011). In all the compounds studied in this work, with the unique exception of NaTlO, whose structure determination is doubtful, the structures of all the ternary alkali oxides and sulfides can be interpreted in terms of the EZKC, a concept that has proved fruitful in spite of the fact that its physical meaning needs wider theoretical support.

The general trend is that one of the alkali metal atoms together with the O (S) atom form four-connected network characteristics of the (IV)–(IV) compounds (Group 14 elements). This idea was applied for the first time to binary and ternary sulfates (Vegas & García-Baonza, 2007), some of which derive from the sulfides studied in this article.

In that article, mainly concerned with sulfates whose cation arrays were of the Ni_2In- and $PbCl_2$-type, as well as in more recent publications devoted to stuffed bixbyites of the formula $Li_3M^{III}N_4$ (Vegas *et al.*, 2009) and $FeLiPO_4$ (Vegas, 2011*b*) it is

clearly illustrated that the simple and fruitful concept enunciated by Zintl (Zintl & Dullenkopf, 1932) is applicable not only to the well known Zintl phases but also to cation arrays in oxides. Recall that also the Al-, Si- and P-skeletons in aluminates, silicates, alumosilicates and silicophosphates are in fact Zintl polyanions if the O atoms are neglected, as has been previously reported (Santamaría-Pérez & Vegas, 2003; Santamaría-Pérez *et al.*, 2005; Santamaría-Pérez & Liebau, 2011).

This idea also finds support in the fact that even in binary oxides/sulfides such as Na_2O/Na_2S, and in the corresponding ternary sulfates such as Na_2SO_4, cations of the same kind, say Na atoms, are separated into two crystallographically independent Wyckoff sites and, as mentioned above, only one of these atoms is involved in the supposed Zintl polyanion, *i.e.* $[NaS]^-$. In quaternary sulfates such as $KNaSO_4$ and in the compounds discussed here, the topological separation of different cations such as Na and K is regarded as normal and gives additional support to our idea, especially when the donor atom coincides with the more electropositive alkali element whereas the most electronegative is that involved in the Zintl polyanion. The structures of RbNaO (Fig. 4) and KNaS (Fig. 7) are clear examples.

This aspect connects with another important issue of crystal structures, that of describing the crystal structures as formed by the addition (intercalation) of blocks of more simple structures. Although some isolated compounds described in this way have been found in the literature since the beginning of crystal chemistry, the most comprehensive study was made by Hyde & Andersson (1989). It should be outlined that this work is not based on cation arrays but rather on cation-centred anion polyhedra, with anions and cations considered in a global manner. So, crystal structures are much more than a set of anions and cations held together in a puzzling manner. On the contrary, they must satisfy several requirements that take place simultaneously and that have been disclosed over the last 25 years.

One of them is the formation of either slabs or blocks with simpler structures. This is the case for some of the structures discussed in this report such as the isotypic compounds RbNaO and KLiS on one hand and $CsLiCl_2$ on the other hand. The former compounds could be formulated as the sum of two components such as [Rb + NaO] and [K + LiS], whilst the latter has a structure consistent with the sum [CsCl + LiCl]. In each case, if one of the constituents is taken out, the full structure of the other is obtained.

This manner of describing the structures was already used for both the Ruddelesen–Popper and the Aurivilius phases, such as K_2MgF_4, as the sum of the two intergrowing slabs, *i.e.* $KF + KMgF_3$ (Hyde & Andersson, 1989).

It is perhaps worth noting that the building blocks are not arbitrary. Some of them have the structure and dimensions of the real phases of metals and/or alloys forming the compound and others can be understood by generalization of the Zintl–Klemm concept, thus producing a useful combination of both concepts which is chemically meaningful. Thus, in RbNaO the structure is the intergrowth of fragments of the Rb metal structure with fragments of composition NaO, which are, in fact, halves of the unit cell of the antifluorite-type Na_2O. In addition, RbNaO can be seen as the result of a charge transfer from Rb to the [NaO] partial structure, leading to $[NaO]^- \equiv \Psi$-MgO, a pseudo-(II)–(VI) compound with the PbO-type structure. We see that both models converge to a more unified vision of the structures.

We have also mentioned that this type of structural feature is maintained when those alloys, for example the binary and ternary sulfides, become the cation arrays of the corresponding oxidized sulfates. The structural identity of the pairs Cs_2S/Cs_2SO_4 and $KNaS/KLiSO_4$ and many others which have been previously reported (Vegas & Jansen, 2002; Vegas & García-Baonza, 2007; Vegas, 2011*a*; Bevan *et al.*, 2011) gives additional support to the general applicability of the EZKC.

A final comment should be made on the crucial question about whether the results we have presented here are the result of mere geometrical arrays mainly governed by the size of classical anions and cations or, on the contrary, they are the consequence of a true electron transfer in the way just described. It is true that some of the charge transfer we have proposed here should be taken as formal. This should be the case for $CsLiCl_2$ or the LiHS phases, but in other cases such as KNaS (see Fig. 7) the electron transfer from K to Na gives a reasonable explanation of the structure, accounting for the observed skeletons. The problem is similar to that presented by either ZnS or AlP where the Si-like structure can only be understood by assuming an electron transfer from the S(P) to the Zn(Al) atoms or by considering that both species contribute eight valence electrons as they do a pair of Si atoms.

We are aware that theoretical calculations will help to solve this controversy and, in this sense, some of them applied to the compounds discussed here are presently in progress. However, it should be noted that previous theoretical calculations carried out on AlX_3 halides (Vegas *et al.*, 2006) as well as the ELF calculations reported for the pairs $BaSn/BaSnO_3$, Ca/CaO and Ca/CaF_2 (Vegas & Mattesini, 2010), and also for high-pressure phase of elemental potassium, the so-called *h*P4-K phase (Marqués *et al.*, 2009), are indications that inorganic solids do not obey many of the principles on which modern crystal chemistry has been based so far.

As reported elsewhere (Vegas *et al.*, 2009) a more profound insight into crystal structures is gained if studies are not restricted to classical anions and cations in their conventional oxidation states, but also to envisage how selected pairs of atoms might accommodate their valence electrons to produce pseudo-structures characteristic of the elements of Group 14. If this is the driving force, the conventional oxidation states assigned to cations and anions lose some of their usefulness in accounting for crystal structures.

References

Albert, B. & Schmitt, K. (1999). *Inorg. Chem.* **38**, 6159–6163.
Aliev, S. A. & Aliev, F. F. (1989). *Inorg. Mater.* **25**, 204–209.
Bach, A., Fischer, D. & Jansen, M. (2009). *Z. Anorg. Allg. Chem.* **635**, 2406–2409.

Bevan, D. J. M., Martin, R. L. & Vegas, A. (2011). *Struct. Bond.* **138**, 93–132.
Blatov, V. A. (2009). http://www.topos.ssu.samara.ru.
Blatov, V. A. (2011). *Struct. Bond.* **138**, 31–66.
Blatov, V. A. & Peskov, M. V. (2006). *Acta Cryst.* B**62**, 457–466.
Borisov, S. V. (2000). *Crystallogr. Rep.* **45**, 709–713.
Bronger, W., Bomba, C. & Sabrowsky, H. (1989). *J. Less-Common Met.* **156**, 43–47.
Catti, M. (2005). *Phys. Rev. B*, **72**, 064105.
Fischer, D., Mueller, A. & Jansen, M. (2004). *Z. Anorg. Allg. Chem.* **630**, 2697–2700.
Gaebell, H. C., Meyer, G. & Hoppe, R. (1983). *Z. Anorg. Allg. Chem.* **498**, 94–98.
Helms, A. & Klemm, W. (1939). *Z. Anorg. Allg. Chem.* **242**, 33–40.
Hofmann, M., Hull, S. & Keen, D. A. (1995). *Phys. Rev. B*, **51**, 12022–12025.
Hyde, B. G. & Andersson, S. (1989). *Inorganic Crystal Structures.* New York: John Wiley.
Inorganic Crystal Structure Database (2010). ICSD. Fachinformationszentrum: Karlsruhe.
Ilyushin, G. D., Blatov, V. A. & Zakutkin, Y. A. (2004). *Z. Kristallogr.* **219**, 468–478.
Jacobs, H., Kirchgassner, R. & Bock, J. (1989). *Z. Anorg. Allg. Chem.* **569**, 111–116.
Juza, R. & Laurer, P. (1954). *Z. Anorg. Allg. Chem.* **275**, 79–93.
Kim, J. & Hughbanks, T. (2000). *Inorg. Chem.* **39**, 3092–3097.
Lebedev, V. I. (1972). *Int. Geol. Rev.* **14**, 543–547.
Liebold-Ribeiro, Y., Fischer, D. & Jansen, M. (2008). *Angew. Chem. Int. Ed.* **47**, 4428–4431.
Mariano, A. N. & Warekois, E. P. (1963). *Science*, **142**, 672–673.
Marqués, M., Ackland, G. J., Lundegaard, L. F., Stinton, G., Nelmes, R. J., McMahon, M. I. & Contreras-García, J. (2009). *Phys. Rev. Lett.* **103**, 115501(4).
Martínez-Cruz, L. A., Ramos-Gallardo, A. & Vegas, A. (1994). *J. Solid State Chem.* **12**, 397.
Nakashima, P. N., Smith, A. E., Etheridge, J. & Muddle, B. C. (2011). *Science*, **331**, 1583–1586.
Nakayama, H., Klug, D. D., Ratcliffe, C. I. & Ripmeester, J. A. (1994). *J. Am. Chem. Soc.* **116**, 9777–9778.
O'Keeffe, M. & Hyde, B. G. (1985). *Struct. Bond.* **61**, 77–144.
Pannetier, G. & Gaultier, M. (1966). *Bull. Soc. Chim. Fr.* pp. 1069–1071.
Parthé, E. & Chabot, B. (1990). *Acta Cryst.* B**46**, 7–23.
Parthé, E. & Engel, N. (1986). *Acta Cryst.* B**42**, 538–544.
Pentin, I. V., Saltykov, V., Nuss, J., Schön, J. C. & Jansen, M. (2012). *Chem. Eur. J.* **18**, 3559–3565.
Rundle, R. E. & Lewis, P. H. (1952). *J. Chem. Phys. A*, **20**, 132–134.
Sabrowsky, H. (1978). *Z. Anorg. Allg. Chem.* **438**, 213–221.
Sabrowsky, H., Mertens, P. & Dönhoff, F. O. (1985). *Z. Naturforsch. B*, **40**, 122–123.
Sabrowsky, H., Thimm, A., Vogt, P. & Harbrecht, B. (1987). *Z. Anorg. Allg. Chem.* **546**, 169–176.
Sabrowsky, H. & Vogt, P. (1987). *Z. Anorg. Allg. Chem.* **553**, 226–230.
Sabrowsky, H., Vogt-Mertens, P. & Thimm, A. (1985). *Z. Naturforsch. B*, **40**, 1761–1762.
Santamaría-Pérez, D. & Liebau, F. (2011). *Struct. Bond.* **138**, 1–29.
Santamaría-Pérez, D. & Vegas, A. (2003). *Acta Cryst.* B**59**, 305–323.
Santamaría-Pérez, D., Vegas, A. & Liebau, F. (2005). *Struct. Bond.* **118**, 121–177.
Santamaria-Perez, D., Vegas, A., Muehle, C. & Jansen, M. (2011). *Acta Cryst.* B**67**, 109–115.
Schneider, A. & Gattow, G. (1954). *Z. Anorg. Allg. Chem.* **277**, 49–59.
Schulz, L. G. (1951). *Acta Cryst.* **4**, 487–489.
Smith, D. K., Cline, C. F. & Austerman, S. B. (1965). *Acta Cryst.* **18**, 393–397.
Sommer, H. & Hoppe, R. (1977). *Z. Anorg. Allg. Chem.* **429**, 118–130.
Staritzky, E. (1956). *Anal. Chem.* **28**, 915.
Svensson, C. (1974). *Acta Cryst.* B**30**, 458–461.
Takemura, K. & Syassen, K. (1982). *Solid State Commun.* **44**, 1161–1164.
Terskikh, V. V., Moudrakovski, I. L., Ratcliffe, C. I., Ripmeester, J. A., Reinhold, C. J., Anderson, P. A. & Edwards, P. P. (2001). *J. Am. Chem. Soc.* **123**, 2891–2892.
Tinkham, M. L. & Dye, J. L. (1985). *J. Am. Chem. Soc.* **107**, 6129–6130.
Vegas, A. (2000). *Crystallogr. Rev.* **7**, 189–286.
Vegas, A. (2011*a*). *Struct. Bond.* **138**, 133–198.
Vegas, A. (2011*b*). *Struct. Bond.* **138**, 67–91.
Vegas, A. & García-Baonza, V. (2007). *Acta Cryst.* B**63**, 339–345.
Vegas, A., Grzechnik, A., Syassen, K., Loa, I., Hanfland, M. & Jansen, M. (2001). *Acta Cryst.* B**57**, 151–156.
Vegas, A. & Jansen, M. (2002). *Acta Cryst.* B**58**, 38–51.
Vegas, A., Martin, R. L. & Bevan, D. J. M. (2009). *Acta Cryst.* B**65**, 11–21.
Vegas, Á. & Mattesini, M. (2010). *Acta Cryst.* B**66**, 338–344.
Vegas, Á., Santamaría-Pérez, D., Marqués, M., Flórez, M., García Baonza, V. & Recio, J. M. (2006). *Acta Cryst.* B**62**, 220–227.
Villars, P. & Cenzual, K. (2008/9). *Pearson's Crystal Data: Crystal Structure Database for Inorganic Compounds* (on CD-ROM), Version 1.0, Release 2008/9. ASM International, Materials Park, Ohio, USA.
Wassermann, B., Hönle, W. & Martin, T. P. (1988). *Solid State Commun*, **65**, 561–564.
Winkler, B., Hytha, M. & Milman, V. (2003). *Phase Trans.* **76**, 187–195.
Winzenick, M., Vijayakumar, V. & Holzapfel, W. B. (1994). *Phys. Rev. B*, **50**, 12381–12385.
Wondratschek, H., Merker, L. & Schubert, K. (1964). *Z. Kristallogr.* **120**, 393–395.
Zintl, E. (1939). *Angew. Chem.* **52**, 1–6.
Zintl, E. & Dullenkopf, W. (1932). *Z. Phys. Chem. Abt. B*, **16**, 195–205.